

CERN-TH-2001-380
 IFUM-700/FT
 FTUAM-01-987

Global analysis of Solar neutrino oscillation evidence including SNO and implications for Borexino

P. Aliani^{a*}, V. Antonelli^{a*}, M. Picariello^{a*}, E. Torrente-Lujan^{abc*}

^a *Dip. di Fisica, Univ. di Milano, and INFN Sezione di Milano,*

Via Celoria 16, Milano, Italy

^b *Dept. Fisica Teorica C-XI, Univ. Autonoma de Madrid, 28049 Madrid, Spain,*

^c *CERN TH-Division, CH-1202 Geneve*

Abstract

An updated analysis of all available neutrino oscillation evidence in Solar experiments including the latest *SNO* data is presented. Predictions for total rates and day-night asymmetry in Borexino are calculated. Our analysis features the use of exhaustive computation of the neutrino oscillation probabilities and the use of an improved statistical χ^2 minimization.

In the framework of two neutrino oscillations we conclude that the best fit to the data is obtained in the LMA region with parameters $(\Delta m^2, \tan^2 \theta) = (5.2 \times 10^{-5} \text{ eV}^2, 0.47)$, $(\chi^2_{min}/n = 0.82, n = 38$ degrees of freedom). Although less favored, solutions in the LOW and VAC regions are still possible with a reasonable statistical significance. The best possible solution in the SMA region gets as maximum a statistical significance as low as $\sim 3\%$.

We study the implications of these results for the prospects of Borexino and the possibility of discriminating between the different solutions. The expected normalized Borexino signal is 0.62 at the best fit LMA solution while the DN asymmetry is negligible (approximately 10^{-5}). In the LOW region the signal is in the range $\sim 0.6 - 0.7$ at 90% confidence level while the asymmetry is $\simeq 1 - 20\%$. As a consequence, the combined Borexino measurements of the total event rate with a error below $\pm 5 - 10\%$ and day-night total rate asymmetry with a precision comparable to the one of SuperKamiokande, will have a strong chance of distinguishing or at least strongly favoring one of the Solar neutrino solutions provided by present data.

* email: paul@lcm.mi.infn.it, vito.antonelli@mi.infn.it, marco.picariello@mi.infn.it, torrente@cern.ch

1 Introduction

Until now, the Solar neutrino problem [1–9] has been defined as the difference between the neutrino flux measured by a variety of Solar neutrino experiments and the predictions of the Standard Solar Model (SSM). This difference can be now explained at the 3σ level by the *SNO* demonstration of the appearance at the Earth of Sun-directed muon and tau neutrino beams and the first determination of the total ${}^8\text{B}$ neutrino flux generated by the Sun [10]. The agreement of this flux with the expectations implies as a by-product the confirmation of the validity of the SSM [11–13].

At present the *SNO* experiment measures the ${}^8\text{B}$ Solar neutrinos through the reactions [14–17]

- 1) Charged Current (CC): $\nu_e + d \rightarrow 2p + e^-$,
- 2) Elastic Scattering (ES): $\nu_x + e^- \rightarrow \nu_x + e^-$.

The first reaction is sensitive exclusively to ν_e neutrinos. The second reaction, the same as the one used in SuperKamiokande (*SK*), is sensitive, with different efficiencies, to all flavors. The *SNO* first results on Solar neutrinos [10], confirm previous evidence from *SK* and other experiments [1, 3, 4, 18]. During 240 days, *SNO* collected 1169 neutrino events. The Solar neutrino flux measured via the observed CC reaction rate, $\phi_{CC}^{SNO} = 1.75 \pm 0.07 \pm 0.12 \pm 10^6 \text{ cm}^{-2} \text{ s}^{-1}$, is lower than the two existing ES reaction rate measurements: the more precise at *SK* $\phi_{ES}^{SK} = 2.32 \pm 0.03 \pm 0.08 \times 10^6 \text{ cm}^{-2} \text{ s}^{-1}$ and that one measured by *SNO* itself $\phi_{ES}^{SNO} = 2.39 \pm 0.34 \pm 0.15 \times 10^6 \text{ cm}^{-2} \text{ s}^{-1}$. Comparison of the ϕ_{CC}^{SNO} and ϕ_{ES}^{SNO} and especially ϕ_{CC}^{SNO} and ϕ_{ES}^{SK} can be considered as the first direct evidence for Solar neutrino oscillations which produce the appearance of muon and tau neutrinos detected at the Earth. When considering only *SNO* results, it is advantageous to use the experimental ratio of CC to ES measurements because of the cancellation of systematic errors. The experimental value is

$$R^{exp} = \phi_{CC}^{SNO} / \phi_{ES}^{SNO} = 0.748 \pm 0.13$$

which is 2σ away from the no-oscillation expectation $R^{exp} = 1$. Recall that the statistical significance of the difference $\phi_{CC}^{SNO} - \phi_{ES}^{SNO}$ is clearly lower ($\sim 1.4\sigma$) [10]. If we use the *ES-SK* result, the no oscillation hypothesis is excluded at $\sim 3.3\sigma$ [19, 50]. Moreover the allowed oscillations to *only* sterile neutrinos is excluded at the same level ($\sim 3\sigma$). Although less favored the oscillations to both active and sterile neutrinos are still allowed [20–26].

Although they are of qualitative importance, the *SNO* results with their large error bars are still far from constraining alone in a significant way the neutrino oscillation parameters. For this purpose we continue to need the data of all other Solar neutrino experiments [1, 2, 4, 27, 28]. The aim of this work is to present an up-to-date analysis of all available Solar neutrino evidence including the latest *CC-SNO* data in a two-neutrino framework. The predictions for day and night signal rates in the near future real time ${}^7\text{Be}$ sensitive Borexino experiment [29–32] are also calculated. Two important characteristics of this paper are the use a thorough numerical computation of the neutrino oscillation probabilities and the use

of an improved χ^2 minimization. We have followed the *SK* standard procedure allowing for a better treatment of correlated uncertainties.

As we show below, the best fit to the full data set including global rates and *SK* energy spectrum is obtained in the *Large Mixing Angle* (LMA) region. Although less favored, solutions in the *Low mass* (LOW) and *Vacuum* (VAC) regions are possible with a reasonable statistical significance. A best fit solution in the *Small Mixing Angle* (SMA) region is strongly disfavored.

This work is organized as follows. In Section 2 we present a summary of the methods that are used: details of the computation of neutrino oscillation probabilities in the Sun and in the Earth, scattering cross sections and calculation of the signal at the detectors. We continue with a detailed account of the χ^2 statistical methods. In Section 3 we present the results of different analyses: first considering total event rates only and then including the *SK* energy spectrum information. In Section 4 we present our Borexino predictions for the best fit solutions obtained in the previous sections. Finally in Section 5 we summarize and draw conclusions.

2 Methods

2.1 Neutrino oscillations and expected signals

In general, our determination of neutrino oscillations in Solar and Earth matter and of the expected signal in each experiment follows the standard methods found in the literature [33]. Nonetheless, this work differs from previous ones in the treatment of the computation of the neutrino transition probabilities. We completely solve numerically the neutrino equations of evolution for all the oscillation parameter space. Although other alternatives as the use of semi-analytical expressions in portions of the $(\Delta m^2, \theta)$ plane could be previously justified in terms of economy of resources, at this stage a full simulation is a better option. For example this becomes necessary in the calculation of the smearing of the neutrino probability as a function of the neutrino production point when introducing non radial propagation.

The survival probabilities for an electron neutrino produced in the Sun to arrive at Earth are calculated in three steps. The propagation from the production point to Sun's surface is computed numerically in all the parameter range using the electron number density n_e given by the BPB 2001 model [12] averaging over the production point. The propagation in vacuum from the Sun surface to the Earth is computed analytically, the averaging over the annual variation of the orbit is also exactly performed using simple Bessel functions. To take the Earth matter effects into account, we have adopted a spherical model of the Earth density and chemical composition. In this model, the Earth is divided in eleven radial density zones [34], in each of which a polynomial interpolation is used to obtain the electron density. The glueing of the propagation of the neutrino in the three different regions is performed exactly using an evolution operator formalism [33]. The final survival

probabilities are obtained from the corresponding (non-pure) density matrices built from the evolution operators in each of these three regions. The night quantities are obtained using appropriate weights which depend on the neutrino impact parameter and the sagitta distance from neutrino trajectory to the Earth center, for each detector's geographical location.

The expected signal in each detector is obtained by convoluting neutrino fluxes, oscillation probabilities, neutrino cross sections and detector energy response functions. We have used neutrino-electron elastic cross sections which include radiative corrections [35]. Neutrino cross sections on deuterium needed for the computation of the *CC-SNO* measurements are taken from [36].

Detector effects are summarized by the respective response functions, obtained by taking into account both the energy resolution and the detector efficiency. The resolution function for *CC-SNO* is that given in Ref. [10]. We obtained the energy resolution function for *SK* using the data presented in Ref. [37–39]. The effective threshold efficiencies, which take into account the live time for each experimental period, are incorporated into our simulation program. They are obtained from Refs. [43].

2.2 The χ^2 calculations: definitions and procedures

The statistical significance of the neutrino oscillation hypothesis is tested with a standard χ^2 method which we explain in some detail here.

In the most simple case, the analysis of global rates presented in Section 3.1, the definition of the χ^2 function is the following:

$$\chi_{\text{glob}}^2 = (\mathbf{R}^{\text{th}} - \mathbf{R}^{\text{exp}})^T (\sigma^2)^{-1} (\mathbf{R}^{\text{th}} - \mathbf{R}^{\text{exp}}) \quad (1)$$

where σ^2 is the full covariance matrix made up of two terms, $\sigma^2 = \sigma_{\text{unc}}^2 + \sigma_{\text{cor}}^2$.

The diagonal matrix σ_{unc}^2 contains the theoretical, statistical and uncorrelated errors while σ_{cor}^2 contains the correlated systematic uncertainties. The $\mathbf{R}^{\text{th,exp}}$ are vectors containing the theoretical and experimental data normalized to the SSM expectations. The length of these vectors is 3 or 4 depending on whether the *CC-SNO* experiment is included or not:

$$R_i^{\text{th,exp}} = S_i^{\text{th,exp}} / S_i^{\text{SSM}}, \quad i = Cl, Ga, SK, (\text{CC-SNO}).$$

The index i denotes the different Solar experiments: Chlorine (*Cl*), Gallium (*Ga*), SuperKamiokande (*SK*) and Charged Current *SNO* (*CC-SNO*).

The correlation matrices, whether including the *SNO* experiment or not, have been computed using standard techniques [40, 41]; our results are summarized in Table (1).

To test a particular oscillation hypothesis $(\Delta m^2, \tan^2 \theta)$ against the parameters of the best fit, we perform a minimization of the χ_{glob}^2 as a function of the oscillation parameters. A point in parameter space $(\Delta m^2, \tan^2 \theta)$ is allowed if the globally subtracted χ_{glob}^2 fulfills the condition $\chi_{\text{glob}}^2(\Delta m^2, \theta) - \chi_{\text{min}}^2 < \chi_n^2(\text{CL})$. Where $\chi_{n=2}^2(90\%, 95\%, \dots) = 4.60, 5.99, \dots$ are the $n = 2$ degrees of freedom quantiles.

A more elaborated statistical analysis is necessary once one introduces the *SK* energy spectrum into the analysis (Section 3.2).

The procedure assumed by the *SK* collaboration, in order to present its own analysis and obtain the tables of bin correlated errors, is that of using the summation $\chi^2 = \sum \chi_i^2$ where each term is of the form [42, 43]

$$\chi_i \sim \alpha f_i(\delta_{\text{cor}}) R_i^{\text{th}} - R_i^{\text{exp}}, \quad (2)$$

and where the expression

$$f_i(\delta_{\text{cor}}) \sim \frac{1}{1 + \sigma_{i,\text{cor}} \delta_{\text{cor}}} \quad (3)$$

is the response function for the correlated error in the i^{th} -energy bin. The $\sigma_{i,\text{cor}}$ are bin-correlated uncertainties and α is an overall normalization factor. The correlation parameter δ_{cor} is arbitrary and determined in the minimization process together with the rest of oscillation parameters.

SuperKamiokande calculation of tables for correlated errors (as Table III in Ref. [43] and previous publications) and the χ^2 prescription given respectively by Eqs. (2) and (3) are closely related. In this work we follow this definition of the χ^2 , however for clarity we write the expressions in a notation which renders the comparison with other published works simple. It can be easily shown that the expression to be presented below lead to the *SK* expressions ¹.

Therefore, for the analysis of the full set of data including *SK* energy spectrum, we consider a χ^2 function which is sum of two quantities $\chi^2 = \chi_{\text{glob}}^2 + \chi_{\text{spec}}^2$. The first one is given by Eq. (1) considering only *Cl*, *Ga* and *CC-SNO* total rates, while for the second term we adopt the definition

$$\chi_{\text{spec}}^2 = \sum_{d,n} (\alpha \mathbf{R}^{\text{th}} - \mathbf{R}^{\text{exp}})^t (\sigma_{\text{unc}}^2 + \delta_{\text{cor}} \sigma_{\text{cor}}^2)^{-1} (\alpha \mathbf{R}^{\text{th}} - \mathbf{R}^{\text{exp}}) + \chi_{\alpha}^2 + \chi_{\delta}^2. \quad (4)$$

A subindex $i = d, n$ corresponding to separated day and night quantities is understood for any \mathbf{R} vector and σ matrix. We have introduced a flux normalization factor α and a correlation parameter δ_{cor} . The complete variance matrix is not a constant quantity. It is obtained from combining the statistical variances with systematic uncertainties and dependent on this correlation parameter.

The corresponding χ^2 terms in Eq. (4) are

$$\chi_{\alpha}^2 = \frac{(\alpha - \alpha^{\text{th}})^2}{\sigma_{\alpha}^2}, \quad \chi_{\delta}^2 = \frac{(\delta_{\text{cor}} - \delta_{\text{cor}}^{\text{th}})^2}{\sigma_{\delta}^2}.$$

The central value $\alpha^{\text{th}} = 1$ corresponds to the BPB ⁸B flux. The uncertainty on α comes from the $^{+19}_{-14}\%$ uncertainty in the, we make an average of the two-side errors and take

¹We have not included a term $\log \det \sigma^2(\delta_{\text{cor}}) \sim \log(1 + \delta_{\text{cor}})$ whose effect is negligible

$\alpha^{\text{th}} \pm \sigma_\alpha = 1.00 \pm 0.17$ [12]. The correlation parameter is assumed to be constrained within σ_δ and we take $\delta_{\text{cor}}^{\text{th}} = 1$.

In this work we consider two cases. In the first case the flux normalization is taken to be free (we allow for a very large $\sigma_\alpha \rightarrow \infty$ in the χ^2_α term). As a second possibility we consider that both quantities α and δ_{cor} are constrained. Note that the unwanted consequence of eliminating the last term χ^2_δ would be to obtain running-away solutions for the optimal value of this parameter.

The χ^2 summation now contains 41 bins in total: 3 from the global rates (all the experiments except *SK*) and 2×19 bins for the *SK* day and night spectrums. The full correlation matrix is defined by blocks. The 3×3 block corresponding to the global rates is defined as above. For each day and night spectrum the corresponding 19×19 block correlation matrices are conservatively constructed assuming full correlation among energy bins ². The components of the variance matrix are

$$\begin{aligned} (\sigma_{\text{cor}}^2)_{ij} &= \sigma_{i,\text{exp}} \sigma_{j,\text{exp}} + \sigma_{i,\text{cal}} \sigma_{j,\text{cal}}, \\ (\sigma_{\text{unc}}^2)_{ii} &= \sigma_{i,\text{stat}}^2 + \sigma_{i,\text{unc}}^2, \end{aligned}$$

where σ_{stat} are the statistic errors and the quantities $\sigma_{\text{exp}}, \sigma_{\text{cal}}, \sigma_{\text{unc}}$ are respectively the bin-correlated experimental, spectrum calculation uncertainties and the bin-uncorrelated ones.

Notice that in the above sum we do not simultaneously include the global ratio for *SK* and the partial spectrum bins. We ignore any correlation between the spectrum information and the global rates of all experiments except *SK* itself. Finally, a remark is in order. In this case the defined covariance matrix is dependent on one of the fitting parameters. One does not, however have to add any correction (i.e. $\log \det \sigma$ terms) to the $\Delta\chi^2$ expression as long as we sit at $\delta_{\text{cor}}^{\text{min}}$. To test a particular oscillation hypothesis and obtain allowed regions in parameter space we perform a minimization of the four dimensional function $\chi^2(\Delta m^2, \tan^2 \theta, \alpha, \delta_{\text{cor}})$. The minimization of the expression with respect to α and δ_{cor} is done analytically. The subsequent minimization in the $(\Delta m^2, \tan^2 \theta)$ plane is numerical. For $\delta_{\text{cor}} = \delta_{\text{cor}}^{\text{min}}, \alpha = \alpha_{\text{min}}$, a given point in the oscillation parameter space is allowed if the globally subtracted quantity fulfills the condition $\Delta\chi^2 = \chi^2(\Delta m^2, \theta) - \chi^2_{\text{min}} < \chi^2_n(CL)$. Where $\chi^2_{n=4}(90\%, 95\%, \dots) = 7.78, 9.4, \dots$ are the quantiles for four degrees of freedom.

3 Results

We have used data on the total event rates measured at Chlorine Homestake experiment, at the gallium experiments *SAGE* [4, 44], *GNO* [27] and *GALLEX* [28] and at the water and heavy-water *SK* (live time 1258 days) [42] and *SNO* (*ES,CC* 240 days [10]) experiments (see Table (2) for an explicit list of results and references).

²The introduction of the parameter δ_{cor} is equivalent to the relaxation of this condition at minimization time.

For the purposes of this work it is enough to summarize all the gallium experiments in one single quantity by taking the weighted average of their rates.

In addition, for *SK* we use the available information for the day and night energy spectrums. For each of the day and night cases, this spectrum information contains 18 total recoil-electron energy bins of width 0.5 MeV in the range 5 to 14 MeV and an additional bin spanning the remaining 14-20 MeV range. The data and errors for individual energy bins for *SK* spectrum has been obtained from Ref. [43]. The information from other *SK* results as the global day night asymmetry is already contained to a large extent in the previous quantities and does not change the results to be presented on continuation [3, 42].

3.1 Global rate analysis

The analysis of the global rates of the four experiments *SK*, Chlorine, Gallium and *CC-SNO* is the simplest possibility but nonetheless it reveals important trends of the solutions to the Solar neutrino problem. It illustrates how the *CC-SNO* data impose additional constraints on the parameter space and in particular how the SMA solution loses its statistical significance in favor of the LMA and LOW regions, becoming allowed only at marginal $3-4\sigma$ confidence levels.

We present results both with and without the inclusion of the *CC-SNO* global rate. In the analysis of the global rates of the *SK*, *Cl*, *Ga* (*CC-SNO*) experiments one has two free parameters Δm^2 and $\tan^2 \theta$ and 3 (4) experimental quantities, therefore the effective number of degrees of freedom (d.o.f.) is 1 (2).

On the left-hand-side of Tables (3-4) we present the best fit parameters or local minima obtained from the minimization of the χ^2 function given in Eq. (1). Also shown are the values of χ^2_{min} per degree of freedom (χ^2/n) and the goodness of fit (g.o.f.) or significance level of each point (definition of SL as in Ref. [45]). On the right-hand-side of the same tables we show the deviations (minimization residuals) from the expected values for all the total event rates. We also include, for further reference, the deviations corresponding to the *SK* day and night energy spectrums and global day-night asymmetry, although these quantities are not incorporated in the χ^2 minimization. We consider first the case in which the *CC-SNO* global rate is ignored. The absolute minimum is located at the SMA region $(\Delta m^2, \tan^2 \theta)^{SMA} = (0.98 \times 10^{-5} \text{ eV}^2, 0.91 \times 10^{-3})$, with $\chi^2_{min}/n = 0.97$ (d.o.f. $n = 3 - 2$), the significance level for this point g.o.f. is 32%. The next local minima are situated at the transition area between LOW and VAC regions $(\Delta m^2, \tan^2 \theta)^{LOW} = (1.28 \times 10^{-8} \text{ eV}^2, 1.64)$, with $\chi^2_{min}/n = 1.25$ and in the LMA region $(\Delta m^2, \tan^2 \theta)^{LMA} = (1.11 \times 10^{-4} \text{ eV}^2, 0.38)$, with $\chi^2_{min}/n = 1.96$ which corresponds to a still reasonable good fit g.o.f. is 16%. The twin VAC regions situated at $(\Delta m^2, \tan^2 \theta)^{VAC} = (9.3(6.4) \times 10^{-10} \text{ eV}^2, 3.05(0.34))$, receive a significance level slightly larger than $\sim 4\%$. For comparison, the much-less significant results corresponding the sterile neutrino oscillation hypothesis are also included in this and following tables.

When one introduces the *CC-SNO* total event rate in the analysis the relative order of the local minima changes. The absolute minimum is now located at the LMA region: $(\Delta m^2, \tan^2 \theta)^{LMA} = (1.11 \times 10^{-4} \text{ eV}^2, 0.42)$. The significance level of the absolute minimum is only slightly worse than in the previous case $\chi^2_{min}/n = 1.16$ (d.o.f. n=4-2) which corresponds to g.o.f. = 31%. After that, we have the pair of minima at the LOW-VAC intermediate region $(\Delta m^2, \tan^2 \theta)^{LOW-VAC} = (1.05 \times 10^{-9} \text{ eV}^2, 2.00(0.42))$, with $\chi^2_{min}/n = 1.22(2.30)$. The significance level of the SMA region is no better than $\chi^2_{min}/n = 2.67$, g.o.f. is 7%, value which is obtained at $(\Delta m^2, \tan^2 \theta)^{SMA} = (0.70 \times 10^{-5} \text{ eV}^2, 1.80 \times 10^{-3})$. Finally, a series of local minima are found on the VAC region with significances above the 4% level.

In Figs. (1) we present graphically our results respectively before and after including the global *CC-SNO* rate. In the plots one can see the regions which are allowed at 90, 95, 99 and 99.743% confidence levels. The main difference between the plots is an overall reduction of the extent of the allowed area at any CL. The large contiguous areas at 3 and 4σ which are present along $\tan^2 \theta \sim 1$ in the first case are converted into well separated patches after the inclusion of *SNO* results. The most serious consequence is however the considerable reduction on the significance of the SMA region. From the analysis of the four global rates this region becomes only acceptable at the $3 - 4\sigma$ level. In these and next plots, the region above the line at high Δm^2 is excluded at 99% CL from the negative results of *CHOOZ* and *Palo Verde* [46]. Note that regions for very large $\Delta m^2 \sim 10^{-3} \text{ eV}^2$ are excluded without need of the *CHOOZ* result once we include the *SNO* result.

The drastic reduction of the SMA region can be explained from the tables of deviation (right part in Tables (3-4)). Before the introduction of the *CC-SNO* global rate in the computation and χ^2 minimization the residuals for the *CC-SNO* data corresponding to the best and second to best fits are very high (Table (3)): respectively 2.9σ for the SMA solution and 4.9σ for the LOW solution. The *CC-SNO* residual values for the following regions are however smaller. When the *CC-SNO* data is incorporated into the fit the SMA and LOW regions become less favored. The effect is much more important for the relatively small SMA region. For the LOW region the initial area is large and nearby minima can be found to adjust for the *CC-SNO* data and still provide reasonable quality fits.

The complicated landscape and the distribution of the minima is graphically shown in Fig. (2). We observe how in the LMA and especially the LOW and VAC regions the different local minima are not clearly separated.

3.2 Day-night *SK* spectra and global rates

In this section we present the results obtained when including the *SK* day and night energy spectrum rates in addition to the total event rates of *Cl*, *Ga* experiments and *CC-SNO*.

The definition of the χ^2 functions and minimization procedures used in the statistical analysis are explained in detail in Section 2.2. The number of experimental data inputs is $2 \times 19 + 3 = 41$. One now has four free parameters, the oscillation parameters Δm^2

and $\tan^2 \theta$, the ${}^8\text{B}$ neutrino flux normalization α and the correlation parameter δ_{cor} . Two cases will be studied. In case A the flux normalization α is considered a free parameter, the number of effective d.o.f. is then $41 - 4 = 37$. In case B, the parameter α is constrained to its BPB 2001 central value within 1σ errors, we now have the d.o.f = 38.

In Tables (5-6) we present the best fit parameters or local minima obtained from the minimization of the χ^2 function given in Eq. (4). As in the previous section, the values of χ^2_{min} per degree of freedom (χ^2/n) and the goodness of fit (g.o.f.) or significance level of all minimal points are shown. In the right part of the tables, the deviations from the expected values or minimization residuals for a number of experimental quantities are listed.

The results for the free flux minimization or case A are presented first. As a summary of numerical results, which appear in detail in Table (5) and Fig. (3, left), the position of the absolute minimum is located at the LMA region $(\Delta m^2, \tan^2 \theta)^{\text{LMA}} = (5.3 \times 10^{-5} \text{ eV}^2, 0.47)$, with $\chi^2_{\text{min}}/n = 0.82$ (d.o.f. n=37). The significance level for this point g.o.f. = 77% is significantly larger, actually twice the significance levels obtained in global rates only analysis. This is only in part an artifact of the statistical machinery. It is a satisfactory result because it basically reflects the internal consistency of the data, although the number of degrees of freedom have considerably increased, the χ^2 per d.o.f is still much the same. The minimization value of the flux normalization is $\alpha = 1.01$ while the correlation parameter is $\delta_{\text{cor}} = 1.40$. The next local minima are situated at the following positions: the LOW region $(\Delta m^2, \tan^2 \theta)^{\text{LOW}} = (1.0 \times 10^{-8} \text{ eV}^2, 1.08)$, with $\chi^2_{\text{min}}/n = 0.90$ and the two solutions at the VAC region $(\Delta m^2, \tan^2 \theta)^{\text{VAC}} = (5.0 \times 10^{-10} \text{ eV}^2, 2.0)$, with $\chi^2_{\text{min}}/n = 1.04$ and $(\Delta m^2, \tan^2 \theta)^{\text{VAC}} = (1.1 \times 10^{-10} \text{ eV}^2, 6.3)$, with $\chi^2_{\text{min}}/n = 1.32$. In this last region the best fit flux normalization is down to $\alpha = 0.7$ while $\delta_{\text{cor}} = 1.85$.

In case B, where the flux normalization is constrained to its SSM value, the results are very similar and are shown in Table (6) and Fig. (3, left). The position of the first minimum remains practically unchanged, the absolute minimum is located at the LMA region $(\Delta m^2, \tan^2 \theta)^{\text{LMA}} = (5.3 \times 10^{-5} \text{ eV}^2, 0.47)$, with $\chi^2_{\text{min}}/n = 0.82$ (d.o.f. n=38) and g.o.f.= 77%. The next local minima are situated at: the LOW region $(\Delta m^2, \tan^2 \theta)^{\text{LOW}} = (0.99 \times 10^{-8} \text{ eV}^2, 1.03)$, with $\chi^2_{\text{min}}/n = 0.86$; and the twin solutions at the VAC region $(\Delta m^2, \tan^2 \theta)^{\text{VAC}} = (5. \times 10^{-10} \text{ eV}^2, 1.86(0.52))$, with $\chi^2_{\text{min}}/n = 1.01$.

In both cases A and B we have a local minimum situated at the SMA region. This minima are situated at approximately $\Delta m^2 \simeq 10^{-5}$ and $\tan^2 \theta$ varying in the range $10^{-4} - 10^{-3}$. The $\chi^2_{\text{min}}/n \simeq 1.3$ gives a very poor statistical significance.

From the Tables (3-4-5-6) and also from the χ^2 landscape shown in Fig. (2) we see that there are some non-negligible regions in parameter space, not only the best fit points. We are therefore justified in converting χ^2 into likelihood using the expression $\mathcal{L} = e^{-\chi^2/2}$, and proceeding to study the marginalized parameter constraints. This normalized marginal likelihood is plotted in Figs. (4) for each of the oscillation parameters Δm^2 and $\tan^2 \theta$. We present results corresponding to two cases: the global rate analysis excluding *CC-SNO* and the full analysis including *SK* energy spectrum. For $\tan^2 \theta$ we observe that the likelihood

function concentrates in a region $0.2 < \tan^2 \theta < 1$ with a clear maximum at $\tan^2 \theta \sim 0.5$ in sharp coincidence with previous results. The situation for Δm^2 is less obvious although the region at large mass differences is clearly favored. The half width of these curves can be used as another estimate of the minimum error which can be assigned to the parameters at the present and near future experimental situation.

4 Borexino implications

The Borexino is a real-time detector for low energy (< 1 MeV) spectroscopy. The experiment's goal is the direct measurement of the ${}^7\text{Be}$ Solar neutrino flux of all flavors via neutrino-electron scattering in an ultra-pure scintillation liquid [29–32].

As before, in order to estimate the Borexino signal one convolutes the Sun neutrino flux with a detector response function which includes the elastic scattering cross sections $\nu_{e,\mu} e^- \rightarrow \nu_{e,\mu} e^-$, energy resolution and energy-dependent efficiency effects. We assume a Gaussian resolution function with an energy dependent width $\sigma(E_{\text{exp}}) = 0.048 \sqrt{E_{\text{exp}}} + 0.01$ MeV. At this stage we suppose unit efficiency over the nominal window of the experiment $0.240 < E < 0.840$ MeV and zero otherwise. The absolute ${}^7\text{Be}$ flux is taken from BPB 2001 [12] as for the other of the experiments. After one year of data taking, the Borexino experiment [51] expects roughly $15 - 20 \times 10^3$ Solar neutrino events with a nearly negligible statistical error $\sigma_{\text{stat}} \sim 0.8\%$. The expected fitting error in discriminating signal from background is much larger $\sigma \sim 8\%$ for the same period of data taking.

In Table (7) and Fig. (5) we present the expectations for the normalized day-night signal $S^{\text{day-night}}$ at the Borexino experiment for any of the local minima solutions found in the previous section (SK spectrum plus global rates with constrained flux): $S^{\text{Bor}} = S^{D-N}(\Delta m^2, \theta)/S_0$ where S_0 is the expected signal in absence of oscillations and day-night signals are averaged. We also present the expected day-night asymmetry $A^{DN} \equiv 2(D - N)/(D + N)$. As we will see below, the asymmetry on the day-night event rates is a valuable tool for distinguishing among the different oscillation solutions. In Fig. (5) we present the expectations for the Borexino experiment as a function of the two-dimensional oscillation parameters. The expected signal varies mildly in ample regions of the parameter space. We observe that at the best fit solution, situated at the LMA region, the expected Borexino normalized signal is $S^{\text{Bor}} = 0.62$. In the whole LMA region (99.7% CL) the signal varies between 0.5 and 0.7. If we restrict ourselves to the 90% CL allowed region around the absolute minimum the signal is always within the range $\sim 0.6 - 0.7$. The asymmetry at the absolute minimum is negligible $A^{DN} < 10^{-5}$, while in the LMA region which surrounds it, it can reach the $\sim 1\%$ level. A similar behavior appears in all the rest of the parameter space except in the LOW region.

In the LOW region the signal varies between $\sim 0.6 - 0.7$ (90% CL). The variation increases to cover the range $\sim 0.5 - 0.8$ at 99.7 CL. Here the day-night asymmetry is expected to be at its maximum. From the table one observes values as high as $A^{DN} \simeq 10 - 20\%$.

In the VAC region the signal varies between $\sim 0.7 - 0.8$. The variation of the expected

signal in the SMA region is much more abrupt. This prevents us from giving accurate predictions for this case. The signal passes from a value $S^{Bor} \sim 0.2$ to $S^{Bor} \sim 0.8$ in a very narrow region. As it is shown in Fig. (6), the combined Borexino measurements of the total event rate with a error below $\pm 7 - 10\%$ and day-night total rate asymmetry with a precision comparable to that one of *SK* will allows us to distinguish or at least to strongly favor the Solar neutrino solutions provided by present data.

5 Conclusions

We have analyzed experimental evidence from all the Solar neutrino data available in this moment including the latest charged current *SNO* results. For the best solutions which fit the present data, we have obtained and analyzed the expectations in Borexino. We considered different combinations of non-redundant data to perform two kinds of analyses: in the first one we only included total event rates for all the experiments, while in the second one we included global rates for Homestake, *GNO-GALLEX-SAGE* and *CC-SNO* plus the day and night energy spectrum rates provided by *SK*. In this last case we studied the possibility of freely or constrained variations of the Boron Solar neutrino flux.

In the simplest case involving global rates only we observed how the inclusion of the *CC-SNO* data causes the decrease of the statistical significance of the SMA solution below the 3σ level.

In the most comprehensive case, global rates plus spectrum, the best fit was obtained in the LMA region with parameters $(\Delta m^2, \tan^2 \theta)^{LMA} = (5.3 \times 10^{-5} \text{ eV}^2, 0.47)$, $(\chi^2_{min}/n = 0.82, \text{d.o.f. } n=38)$. Solutions in the LOW and VAC regions are still possible although much less favored. The best possible solution in the SMA region gets a low statistical significance.

We have analyzed the expectations on the future experiment Borexino in detail for all the favored neutrino oscillation solutions. The expected Borexino normalized signal is $S^{Bor} = 0.62$ at the best fit LMA solution while the day night asymmetry is negligible $A^{DN} < 10^{-5}$. In the VAC region the signal is slightly higher $\sim 0.7 - 0.8$ and the asymmetry is still practically negligible. In the whole LMA region (99.7% CL) the signal varies between 0.5 and 0.7. In the LOW region the signal is in the range $\sim 0.6 - 0.7$ at 90% CL while the asymmetry $A^{DN} \simeq 1 - 20\%$. We conclude that in the near future after 2-3 years of data taking the combined Borexino measurements of the total event rate with an error below $\pm 5 - 10\%$ and day-night total rate asymmetry with a precision comparable to that of *SK* will allows us to distinguish or at least to strongly favor the Solar neutrino solutions provided by present data.

Acknowledgments

It is a pleasure to thank R. Ferrari for many enlightening discussions and for his encouraging support without which this work would have not been possible. We thank all the Borexino

group of Milano University and especially M. Giammarchi, S. Bonetti and B. Caccianiga for providing us essential information about the experiment and its signal discrimination power. One of us (V.A.) would like to thank M. Pallavicini for interesting and useful discussions about Borexino features and potentiality. We acknowledge the financial support of the Italian MIUR, the Spanish CYCIT funding agencies and the CERN Theoretical Division. The numerical calculations have been performed in the computer farm of the Milano University theoretical group.

References

- [1] R. Davis, Prog. Part. Nucl. Phys. 32 (1994) 13. B.T. Cleveland et al., (HOMESTAKE Coll.) Nucl. Phys. (Proc. Suppl.) **B 38** (1995) 47. B.T. Cleveland et al., (HOMESTAKE Coll.) *Astrophys. J.* 496 (1998) 505-526.
- [2] Y. Fukuda *et al.* [Super-Kamiokande Collaboration], *Phys. Rev. Lett.* **82**, 2430 (1999) [arXiv:hep-ex/9812011].
- [3] Y. Fukuda *et al.* [Super-Kamiokande Collaboration], *Phys. Rev. Lett.* **82**, 1810 (1999) [arXiv:hep-ex/9812009].
- [4] J.N. Abdurashitov et al. (SAGE Coll.) *Phys. Rev. Lett.* 83(23) (1999) 4686.
- [5] P. Langacker. Talk given at 4th Intl. Conf. on Physics Beyond the Standard Model, Lake Tahoe, CA, 13-18 Dec. 1994, hep-ph/9503327; Published in Trieste HEP Cosmol.1992:0487-522. *Ibid.*, Nucl. Phys. (Proc. Suppl.) **B 77** (1999) 241, hep-ph/9811460. *Ibid.*, Talk given at 1th Int. Workshop on Weak Interactions and neutrinos (WIN99), Cape Town, SA, 24-30 Jan 1999, hep-ph/9905428.
- [6] P. Ramond, hep-ph/9809401, Nucl. Phys. (Proc. Suppl.) **B 77** (1999) 3.
- [7] F. Wilczek, hep-ph/9809509, Nucl. Phys. (Proc. Suppl.) **B 77** (1999) 511.
- [8] S.M. Bilenky et al. Summary of the Europhysics neutrino Oscillation Workshop Amsterdam, The Netherlands, 7-9 Sep 1998, hep-ph/9906251. S.M. Bilenky, C. Giunti and C.W. Kim, hep-ph/9902462, *Int.J.Mod.Phys.A***15**(2000) 625.
- [9] E. Torrente-Lujan, arXiv:hep-ph/9902339.
- [10] Q. R. Ahmad *et al.* [SNO Collaboration], *Phys. Rev. Lett.* **87** (2001) 071301 [arXiv:nucl-ex/0106015].
- [11] S. Turck-Chieze, *Nucl. Phys. Proc. Suppl.* **91** (2001) 73.
E. G. Adelberger *et al.*, *Rev. Mod. Phys.* **70** (1998) 1265 [arXiv:astro-ph/9805121].
A. S. Brun, S. Turck-Chieze and P. Morel, arXiv:astro-ph/9806272.
- [12] J. N. Bahcall, M. H. Pinsonneault and S. Basu, *Astrophys. J.* **555**, 990 (2001) [arXiv:astro-ph/0010346].
- [13] J.N. Bahcall and M.H. Pinsonneault, *Rev. Mod. Phys.* **67** (1995) 781.
- [14] J. R. Klein [SNO Collaboration], *In *Venice 1999, Neutrino telescopes, vol. 1** 115-125.
A. B. McDonald [SNO Collaboration], *Nucl. Phys. Proc. Suppl.* **77** (1999) 43.

- [15] J. Boger *et al.* [SNO Collaboration], Nucl. Instrum. Meth. A **449** (2000) 172 [arXiv:nucl-ex/9910016].
- [16] V. Barger, D. Marfatia and K. Whisnant, Phys. Lett. B **509** (2001) 19 [arXiv:hep-ph/0104166].
- [17] J. N. Bahcall, P. I. Krastev and A. Y. Smirnov, JHEP **0105** (2001) 015 [arXiv:hep-ph/0103179].
- [18] Y. Fukuda *et al.* [Super-Kamiokande Collaboration], Phys. Rev. Lett. **81**, 1158 (1998) [Erratum-ibid. **81**, 4279 (1998)] [arXiv:hep-ex/9805021].
- [19] A. W. Poon [SNO Collaboration], arXiv:nucl-ex/0110005.
- [20] V. Barger, D. Marfatia and K. Whisnant, arXiv:hep-ph/0106207.
- [21] G. L. Fogli, E. Lisi, D. Montanino and A. Palazzo, Phys. Rev. D **64** (2001) 093007 [arXiv:hep-ph/0106247].
- [22] P. I. Krastev and A. Y. Smirnov, arXiv:hep-ph/0108177.
- [23] J. N. Bahcall, M. C. Gonzalez-Garcia and C. Pena-Garay, JHEP **0108**, 014 (2001) [arXiv:hep-ph/0106258].
- [24] A. Bandyopadhyay, S. Choubey, S. Goswami and K. Kar, arXiv:hep-ph/0110307.
- [25] S. Choubey, S. Goswami and D. P. Roy, arXiv:hep-ph/0109017.
- [26] A. Bandyopadhyay, S. Choubey, S. Goswami and K. Kar, Phys. Lett. B **519** (2001) 83 [arXiv:hep-ph/0106264].
- [27] M. Altmann et al. (GNO Coll.) Phys. Lett. B490 (2000) 16-26.
- [28] P. Anselmann et al., GALLEX Coll., Phys. Lett. **B 285** (1992) 376. W. Hampel et al., GALLEX Coll., Phys. Lett. **B 388** (1996) 384. T.A. Kirsten, Prog. Part. Nucl. Phys. 40 (1998) 85-99. W. Hampel et al., (GALLEX Coll.) Phys. Lett. **B 447** (1999) 127. M. Cribier, Nucl. Phys. (Proc. Suppl.) **B 70** (1999) 284. W. Hampel et al., (GALLEX Coll.) Phys. Lett. **B 436** (1998) 158. W. Hampel et al., (GALLEX Coll.) Phys. Lett. **B 447** (1999) 127.
- [29] T. Hagner [BOREXINO Collaboration], Part. Nucl. Lett. **104**, 90 (2001).
- [30] S. M. Bilenky, T. Lachenmaier, W. Potzel and F. von Feilitzsch, arXiv:hep-ph/0109200.
- [31] C. Arpesella *et al.* [BOREXINO Collaboration], arXiv:hep-ex/0109031.
- [32] E. Meroni, Nucl. Phys. Proc. Suppl. **100**, 42 (2001).

- [33] E. Torrente-Lujan, Phys. Rev. **D 59** (1999) 093006. E. Torrente-Lujan, Phys. Rev. **D 59** (1999) 073001. E. Torrente-Lujan, Phys. Lett. **B 441** (1998) 305. V.B. Semikoz, E. Torrente-Lujan, Nucl. Phys. **B 556** (1999) 353. E. Torrente-Lujan, Phys. Lett. **B494** (2000) 255 [hep-ph/9911458].
- [34] I. Mocioiu and R. Shrock, Phys. Rev. D **62** (2000) 053017 [arXiv:hep-ph/0002149].
A. Dziewonski, in *The Encyclopedia of Solid Earth Geophysics*, edited by D.E James (Van Nostrand Reinhold, New York 1989).
- [35] J. Bahcall, M. Kamionkowski, A. Sirlin, Phys. Rev. D51 (1995) 6146.
- [36] S. Nakamura, T. Sato, V. Gudkov and K. Kubodera, Phys. Rev. C **63** (2001) 034617 [arXiv:nucl-th/0009012].
- [37] H. Ishino, Ph. D. thesis, University of Tokio, 1999.
M. Nakahata et al. (SK Coll.), Nucl. Instrum. Methods 46 (1998) 301.
- [38] M. Nakahata *et al.* [Super-Kamiokande Collaboration], Nucl. Instrum. Meth. A **421**, 113 (1999) [arXiv:hep-ex/9807027].
- [39] N. Sakurai, Ph.D. Thesis, Dec. 2000 *Constraints of the neutrino oscillation parameters from 1117 day observation of solar neutrino day and night spectra in Super-Kamiokande*.
- [40] G. L. Fogli and E. Lisi, Astropart. Phys. **3** (1995) 185.
- [41] S. Goswami, D. Majumdar and A. Raychaudhuri, Phys. Rev. D **63** (2001) 013003 [arXiv:hep-ph/0003163].
- [42] S. Fukuda *et al.* [Super-Kamiokande Collaboration], Phys. Rev. Lett. **86**, 5656 (2001) [arXiv:hep-ex/0103033].
- [43] S. Fukuda *et al.* [SKamiokande Collaboration], Phys. Rev. Lett. **86**, 5651 (2001) [arXiv:hep-ex/0103032].
- [44] A.I. Abazov et al. (SAGE Coll.), Phys. Rev. Lett. **67** (1991) 3332. D.N. Abdurashitov et al. (SAGE Coll.), Phys. Rev. Lett. **77** (1996) 4708. J.N. Abdurashitov et al., (SAGE Coll.), Phys. Rev. **C60** (1999) 055801; astro-ph/9907131. J.N. Abdurashitov et al., (SAGE Coll.), Phys. Rev. Lett. **83** (1999) 4686; astro-ph/9907113.
- [45] D. E. Groom *et al.* [Particle Data Group Collaboration], Eur. Phys. J. C **15** (2000) 1.
- [46] M. Apollonio et al. (CHOOZ coll.), hep-ex/9907037, Phys. Lett. **B 466** (1999) 415. M. Apollonio *et al.*, Phys. Lett. **B 420** (1998) 397.
F. Boehm *et al.*, Phys. Rev. **D62** (2000) 072002 [hep-ex/0003022].

- [47] J. Burguet-Castell and O. Mena, arXiv:hep-ph/0108109.
- [48] K. Lande (For the Homestake Coll.) Nucl. Phys. B(Proc. Suppl.)77(1999)13-19.
- [49] J.N. Bahcall, P.I. Krastev and E. Lisi, Phys. Rev. C **55**, 494 (1997);
B. Faid, G.L. Fogli, E. Lisi and D. Montanino, Astropart. Phys. **10**, 93 (1999).
- [50] V. Berezinsky, arXiv:hep-ph/0108166.
- [51] M. Giammarchi (Borexino Coll.), private communication

	<i>Cl</i>	<i>Ga</i>	<i>SK</i>	<i>CC-SNO</i>
<i>Cl</i>	1.00	0.63	0.62	0.60
<i>Ga</i>		1.00	0.97	0.95
<i>SK</i>			1.00	0.97
<i>CC-SNO</i>				1.00

Table 1: Table of statistical correlations among the total event rates of Homestake (*Cl*), the averaged *SAGE+GALLEX+GNO* (*Ga*), SuperKamiokande (*SK*) and the charged current *SNO* (*CC-SNO*).

Experiment [Ref.]	S_{SSM}	$S_{Data}/S_{SSM} (\pm 1\sigma)$
<i>SK</i> (1258d) [42]	$2.32 \pm 0.03 \pm 0.08$	0.451 ± 0.011
<i>CC-SNO</i> (240d, 8-20 MeV) [10]	$2.39 \pm 0.34 \pm 0.15$	0.347 ± 0.029
<i>Cl</i> [48]	$2.56 \pm 0.16 \pm 0.16$	0.332 ± 0.056
<i>SAGE</i> [4, 44]	$67.2 \pm 7.0 \pm 3.2$	0.521 ± 0.067
<i>GNO-GALLEX</i> [27, 28]	$74.1 \pm 6.7 \pm 3.5$	0.600 ± 0.067

Table 2: Summary of data used in this work. The expected signal (S_{SSM}) and observed ratios S_{Data}/S_{SSM} with respect to the BPB 2001 model are reported. The *SK* and *CC-SNO* rates are in $10^6 \text{ cm}^{-2} \text{ s}^{-1}$ units. The *Cl*, *SAGE* and *GNO-GALLEX* measurements are in SNU units. The results of *SAGE* and *GNO-GALLEX* are combined for its use in this work: S_{Ga}/S_{SSM} ($Ga \equiv SAGE+GALLEX+GNO$) = 0.579 ± 0.050 . The ${}^8\text{B}$ total flux is taken from the BPB 2001 model [12]: $\phi_\nu({}^8\text{B}) = 5.05(1^{+0.20}_{-0.16}) \times 10^6 \text{ cm}^{-2} \text{ s}^{-1}$.

Solution	Δm^2	$\tan^2 \theta$	χ^2_m/n	g.o.f.	<i>SK</i>	<i>Cl</i>	<i>Ga</i>	<i>SNO</i>	A_{SK}^{DN}	Sp^{DN}
SMA	9.8×10^{-4}	0.91×10^{-3}	1.0	32	0.6	0.7	0.2	2.9	1.2	2.4
VAC-LOW	1.3×10^{-8}	1.60	1.2	26	0.1	0.9	0.4	4.9	1.3	2.6
LMA	1.1×10^{-4}	0.38	2.0	16	0.0	1.3	0.3	0.5	1.1	0.8
VAC	9.3×10^{-10}	3.05	3.9	4.5	2.0	1.9	1.0	1.6	1.3	4.7
VAC	6.4×10^{-10}	0.34	4.2	4.0	0.3	1.8	0.5	1.4	1.3	2.8
SMA(ster.)	2.3×10^{-5}	1.23×10^{-3}	5.6	3.2	1.0	0.6	2.8	1.5	2.7	2.4
VAC(ster.)	3.3×10^{-10}	0.49	5.7	3.2	2.5	2.3	1.8	0.7	1.2	2.5

Table 3: (Left) Best fit oscillation parameters: Δm^2 (eV 2) and $\tan^2 \theta$, from the analysis of global rates: *Cl*, *Ga* and *SK*. The *SNO* measurement is not included (d.o.f. = 3 – 2). The significance level g.o.f. is in percentage. The sampling error is $\sim 3\%$ for Δm^2 and $\sim 5\%$ for $\tan^2(\theta)$. For comparison, the results corresponding to the sterile neutrino oscillation hypothesis are included at the end. (Right) Minimization residuals in 1σ units for diverse experimentally measured quantities: the global rates for the four experiments and for *SK* alone the global day-night asymmetry (A^{DN}) and the sum of day and night energy spectrums (Sp^{DN}). Only the first three quantities appear in the χ^2 computation.

Solution	Δm^2	$\tan^2 \theta$	χ^2_m/n	g.o.f.	SK	Cl	Ga	SNO	A_{SK}^{DN}	Sp_{SK}^{DN}
LMA	1.1×10^{-4}	0.42	1.2	31	0.2	1.4	0.5	0.1	1.3	0.8
VAC-LOW	1.0×10^{-9}	2.00	1.2	29	1.2	1.7	0.1	0.3	1.3	1.7
VAC-LOW	1.0×10^{-9}	0.42	2.3	10	1.9	1.9	1.2	1.1	1.3	1.3
LOW	1.3×10^{-7}	0.64	2.6	7.0	1.3	1.8	1.5	1.5	0.3	0.8
SMA	6.7×10^{-6}	1.80×10^{-3}	2.7	6.8	1.8	1.9	0.3	0.0	5.5	5.3
VAC	2.3×10^{-10}	1.40	2.8	6.2	2.3	2.2	1.0	3.1	1.3	4.5
VAC	7.7×10^{-11}	0.31	3.2	4.2	0.5	2.4	0.8	0.3	1.3	2.8
VAC	6.4×10^{-11}	2.70	3.3	3.6	0.7	1.6	0.5	1.0	1.3	3.1
SMA(ster.)	3.7×10^{-5}	1.20×10^{-3}	7.6	3.2	1.2	1.1	2.1	1.1	2.7	3.4
VAC(ster.)	4.1×10^{-10}	0.37	6.1	4.5	1.5	2.4	1.9	1.2	1.3	2.4

Table 4: Best fit oscillation parameters, Δm^2 (eV 2) and $\tan^2 \theta$, and minimization residuals (see explanation in Table 3). The analysis includes now the global rates for the four experiments: Cl , Ga , SK and $CC-SNO$ (d.o.f. = 4 – 2).

Solution	Δm^2	$\tan^2 \theta$	χ^2_{min}/n	g.o.f.	SK	Cl	Ga	SNO	A_{SK}^{DN}	Sp^{DN}
LMA	5.2×10^{-5}	0.47	0.8	77	0.4	0.9	1.1	0.5	0.9	1.0
LOW	9.9×10^{-9}	1.0	0.9	71	3.1	2.6	0.6	3.3	1.2	1.0
LOW	7.7×10^{-8}	0.88	0.9	66	3.3	2.9	0.1	3.9	0.3	0.8
LMA	1.1×10^{-5}	0.88	0.9	58	2.9	2.3	1.8	3.1	1.3	1.0
VAC	5.0×10^{-10}	2.0	1.04	40	5.1	3.6	0.2	5.0	1.3	0.4
SMA	9.8×10^{-6}	1.2×10^{-04}	1.3	11	11	5.1	1.6	11	3.1	0.6
VAC	1.1×10^{-10}	6.3	1.3	11	8.7	5.9	2.7	7.4	1.3	0.4
LMA(ster.)	3.1×10^{-5}	0.67	0.9	45	3.1	2.6	1.9	3.6	2.0	1.1
VAC(ster.)	5.5×10^{-10}	3.2	1.1	37	4.7	2.8	0.2	5.7	1.2	0.5

Table 5: Best fit oscillation parameters, Δm^2 (eV 2) and $\tan^2 \theta$, and minimization residuals (see explanation in Table 3). The analysis includes now the global rates for three experiments Cl , Ga and $CC-SNO$, and SK day and night energy spectra. There are four parameters: Δm^2 , $\tan^2 \theta$, α and δ_{cor} . We let the flux normalization α vary freely, so the d.o.f is = 41 – 4 (see the text). The sampling error due to the finite-grid is $\sim 10\%$ for Δm^2_{min} and $\sim 5\%$ for $\tan^2(\theta)$.

Solution	Δm^2	$\tan^2(\theta)$	χ^2_{min}/n	g.o.f.	SK	Cl	Ga	SNO	A_{SK}^{DN}	Sp^{DN}
LMA	5.2×10^{-5}	0.47	0.8	77	0.4	0.9	1.1	0.5	0.9	1.0
LOW	9.9×10^{-9}	1.03	0.9	65	3.1	2.6	0.6	3.3	1.2	1.0
LOW	1.3×10^{-7}	0.64	0.9	60	1.3	1.8	1.5	1.5	0.3	0.8
LOW	3.6×10^{-8}	0.97	0.9	60	3.5	2.8	0.3	3.9	1.0	0.9
LMA	4.6×10^{-6}	1.42	1.0	35	6.2	4.4	0.1	6.6	0.4	1.0
VAC	5.0×10^{-10}	1.86	1.1	28	4.8	3.3	0.1	4.6	1.3	0.3
VAC	5.0×10^{-10}	0.52	1.1	24	4.9	3.3	0.7	4.7	1.3	0.3
SMA	5.6×10^{-6}	1.32×10^{-3}	1.4	3.2	2.3	0.1	1.4	4.2	1.0	0.9
LMA(ster.)	5.1×10^{-6}	2.09	1.1	29	5.2	4.4	0.7	5.3	0.5	1.3
LOW(ster.)	3.8×10^{-8}	1.27	1.2	17	3.5	3.2	0.5	4.1	1.1	1.2

Table 6: Same as Table 5 except that here the flux normalization α is constrained to vary within its SSM standard error and the d.o.f is = 41 – 4 (see the text).

Solution	$\Delta m^2(\text{eV}^2)$	$\tan^2(\theta)$	S^{Bor}	A_{Bor}^{DN} (%)
LMA	5.2×10^{-5}	0.47	0.62	0.00
LOW	9.9×10^{-9}	1.03	0.62	1.20
LOW	7.7×10^{-8}	0.88	0.64	27.9
LMA	1.1×10^{-5}	0.88	0.58	-1.7
VAC	5.0×10^{-10}	2.0	0.64	0.06

Table 7: Borexino experiment expectations for the normalized total signal (S^{Bor}) and day-night asymmetry (A^{DN}) for any of the best fit solutions appearing in Table (5).

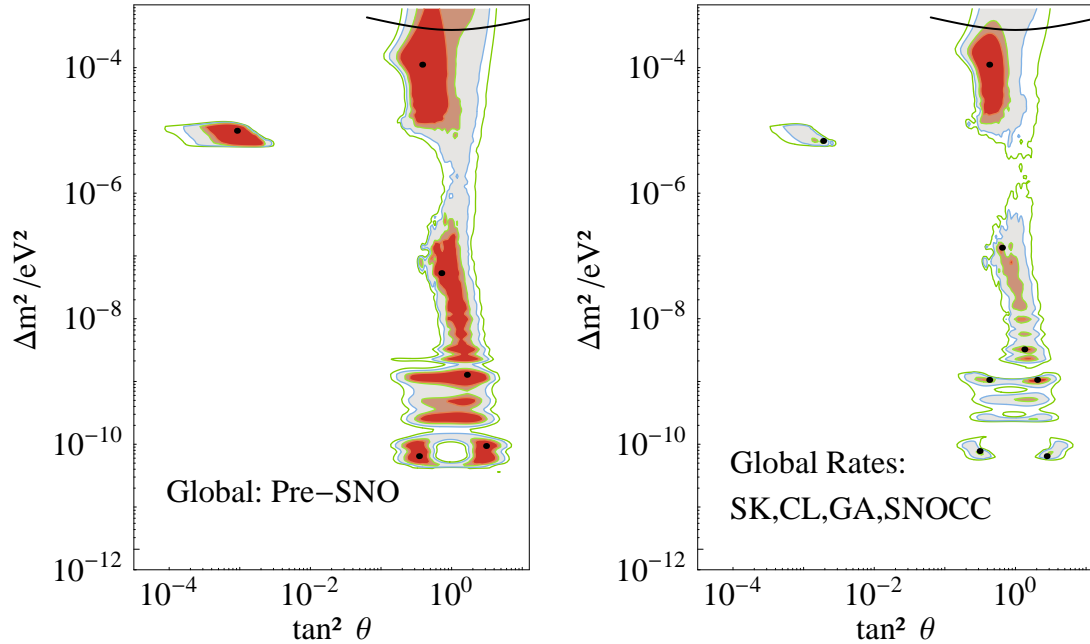


Figure 1: Best fit solutions for the global rate analysis. Global rates from *SK*, *Cl* and *Ga* experiments are included. The right figure contains also the *CC-SNO* one. The black dots are the best fit points (the absolute minimum is located at the SMA (left) or LMA (right) regions). The colored areas are the allowed regions at 90, 95, 99 and 99.7% CL relative to the absolute minimum. The region above the solid line is excluded by *CHOOZ* results at 99% CL [46].

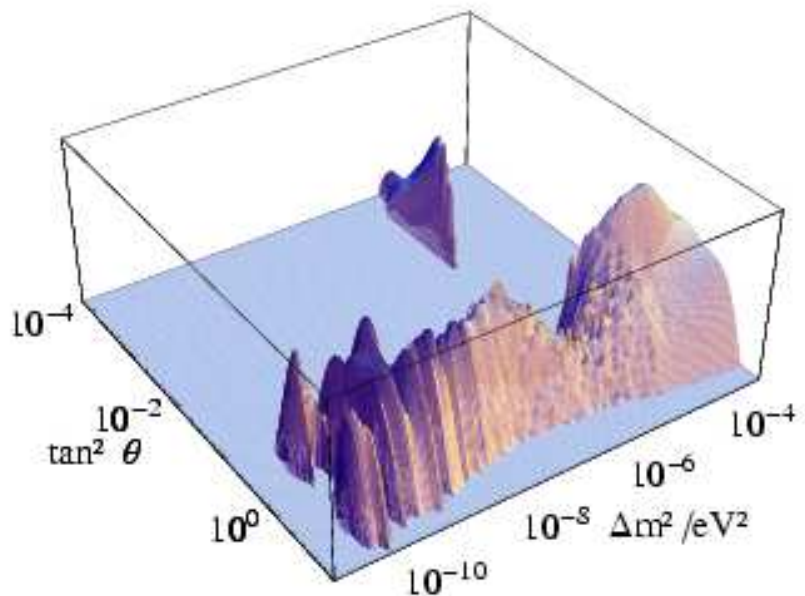


Figure 2: The quantity $-\chi^2$ as a function of the oscillation parameters ($\Delta m^2, \tan^2 \theta$). The scales are logarithmic. Notice the negative sign: the best fit solutions correspond to the maxima in this plot.

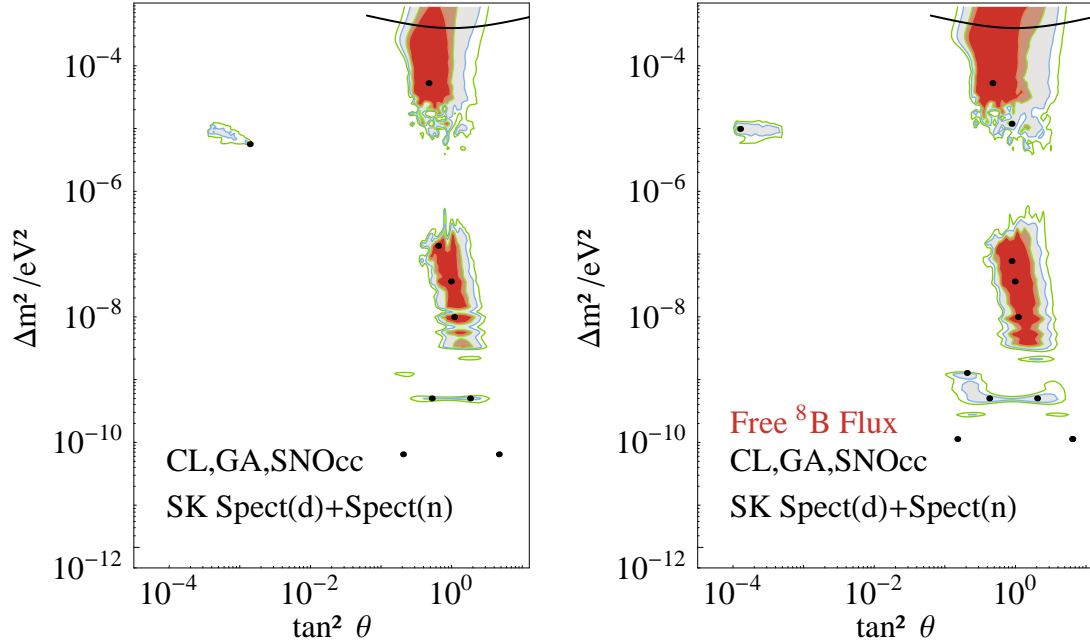


Figure 3: Global solutions for the analysis of *Cl*, *Ga* and *CC-SNO* experiments plus the day-night *SK* spectrum rates. The black dots correspond to best fit points. The colored areas are the allowed regions at 90, 95, 99 and 99.7% CL relative to the absolute minimum. Left (case A of the Text): the absolute normalization factor α and correlation parameter δ_{cor} are varied subject to constraints. Right (case B of the text): the minimization with respect δ_{cor} is performed as before. The absolute normalization factor α is left to vary freely.

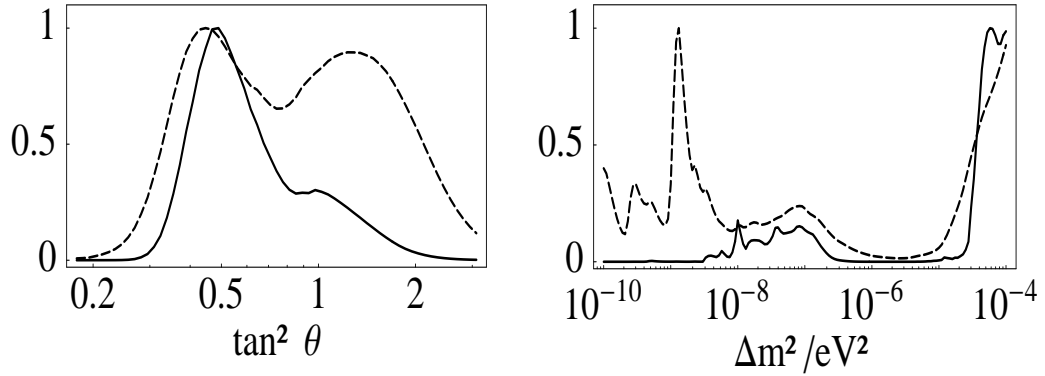


Figure 4: Marginalized likelihood distributions for each of the oscillation parameters Δm^2 (right), $\tan^2 \theta$ (left) appearing in the χ^2 fit. The curves are in arbitrary units with normalization to the maximum height. The continuous lines shows the distributions corresponding to Fig. (3, right). Dashed lines correspond to the case represented in Fig. (3, left).

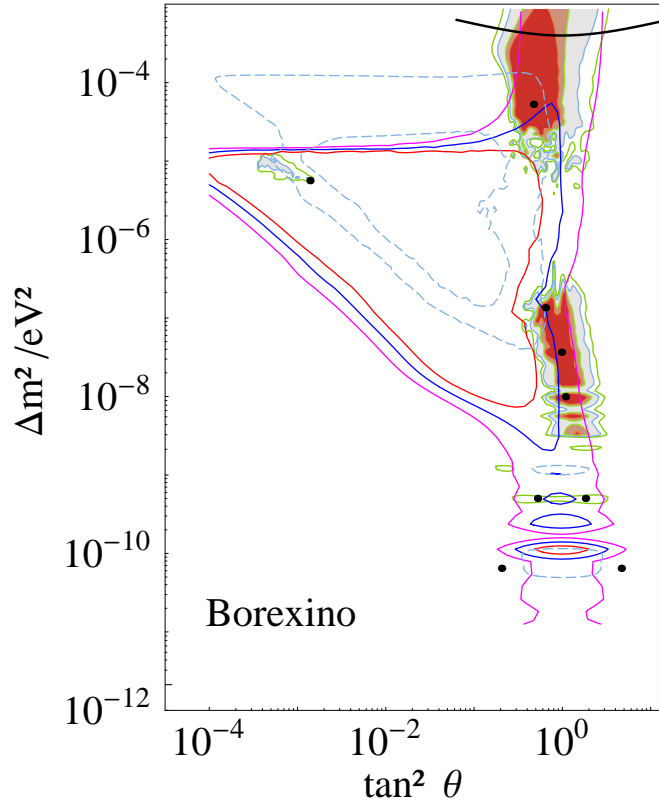


Figure 5: The signal at the Borexino experiment as a function of the oscillation parameters. The signal is normalized to the no-oscillation case. Contours are drawn at $S/S_0 = 0.5, 0.6, 0.7$ with full lines (respective from inside to outside). Superimposed: the allowed regions from the global rate analysis including *CC-SNO* (see Fig. (3), left) and the 1σ allowed regions (here included between the dashed lines) from the ^{18}Be sensitive *Cl* experiment alone.

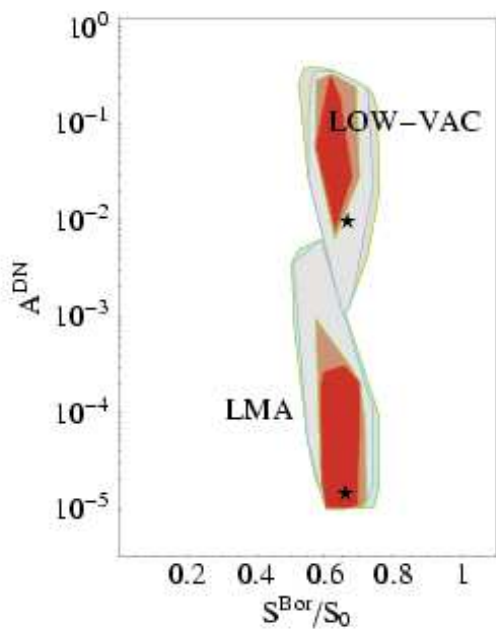


Figure 6: Day night asymmetry $|A^{DN}|$ versus normalized signal at Borexino corresponding to the 90, 95, 99, 99.7 % CL allowed regions from the full analysis including global rates and SK spectra. The upper (lower) zones correspond to the LOW and VAC (LMA) regions in Fig. (3, left). The stars are the expectations of the best fit solutions in each of the regions.